ISSN (online): 2349-784X

A Three-Phase Multilevel Inverter using Limited Power Electronic Components

Krishna Mohan Das

Assistant Professor Einstein Academy of Technology & Management, Odisha B. Krishnapriya

Assistant Professor Einstein Academy of Technology & Management, Odisha

Binaya Kumar Malika

Assistant Professor Einstein Academy of Technology & Management, Odisha

Abstract

In this paper, a three-phase five-level voltage-source inverter is introduced with a new configuration. The proposed inverter constitutes of a conventional three-phase two-level bridge with three bi-directional switches. A multi-level dc-link using constant dc voltage supply and cascaded half-bridge is associated (linked) in such a way that the proposed inverter gives us the required output voltage levels. For the purpose of increasing the number of voltage levels with optimized number of power electronic components, it is recommended to use different methods to determine the magnitudes of utilized dc voltages. The important frequency staircase modulation method is easily used to generate the suitable switching gate signals. Moreover, the model type of the advised configuration can be manufactured as the obtained hardware & simulation results ensures its feasibility of the configuration and the compatibility of the modulation technique is precisely noted.

Keywords: Bidirectional Switch, Fundamental Frequency Staircase Modulation, Multilevel Inverter

I. INTRODUCTION

MULTI-LEVEL inverters comprises of a group of switching devices and dc supply voltages, which produces output voltages with stepped waveforms. Multi-level technology has started with the three-level converter followed by numerous multi-level converter topologies. Many distinct topologies and wide variety of control methods have been developed in the recent literatures. The common multi-level inverter configurations are Cascaded Hybrid Bridge (CHB), Neutral Point Clamped (NPC) and Flying Capacitor (FC). The unbalanced voltage in the dc link of FC, the deviating voltage of Neutral Point voltage in NPC, and the huge number of separated dc supplies in CHB are considered the main problems of these topologies. Apart from these three main topologies, few other topologies were introduced. Recently, hybrid multistage & asymmetrical topologies are becoming one of the utmost interested research area. The hybrid multistage converters comprises of different multi-level configurations with unequal dc supply voltages, whereas, in asymmetrical topologies, the magnitudes of dc supply voltages are unequal. These topologies not only reduces the cost but also improves the reliability and decreases the size of the inverters, because of the use of minimum number of power electronic components, capacitors, and dc supplies. With such inverters, different modulation strategies and power electronic technologies are required.

On the other hand, in order to improve the performance of the conventional single phase and three-phase inverters, different topologies using different types of bi-directional switches have been advised. Comparing to the unidirectional one, bi-directional switch is able to conduct the current and withstand the voltage in both directions. Bi-directional switches with a suitable control technique can enhance the performance of the multi-level inverters in terms of reducing the number of semiconductor devices, optimizing the withstanding voltage and achieving the desired output voltage with higher levels. Based upon this technical background, this paper suggests a topology for a three-phase five-level multi-level inverter. As the number of insulated-gate driver circuits, switching devices are minimized, so the installation area and cost also reduces significantly. The magnitudes of the utilized dc supply voltages have been selected in a way that increases the number of voltage levels with an effective application of a fundamental frequency staircase modulation technique. Extended structure for N-level is also presented and compared with the conventional well-known multilevel inverters. Hardware & Simulation results are given and explained.

II. PROPOSED TOPOLOGY

The typical configuration of the proposed three-phase five-level multilevel inverter is shown in Fig. 1(a) and (b). Three bidirectional switches (S1-S6, Da1-Dc2), two switches, two diodes type, are added to the conventional three-phase two-level bridge (Q1-Q6). The main work of these bi-directional switches is to block the higher voltage and ease current flow to and from the midpoint (o). A multi-level dc link built by a single dc supply voltage with fixed magnitude of 4Vdc and Cascaded Hybrid Bridge having two unequal dc supply voltages of Vdc and 2Vdc are connected to (+, -, o) bridge terminals. Based upon the required number of output voltage levels, a number of Cascaded Hybrid Bridge cells are used. Since the proposed inverter is designed to

achieve five voltage levels, the power circuit of the Cascaded Hybrid Bridge makes use of two series cells having two unequal dc supply voltages.

In each cell, the two switches are turned ON and OFF under inverted conditions to output two different voltage levels.

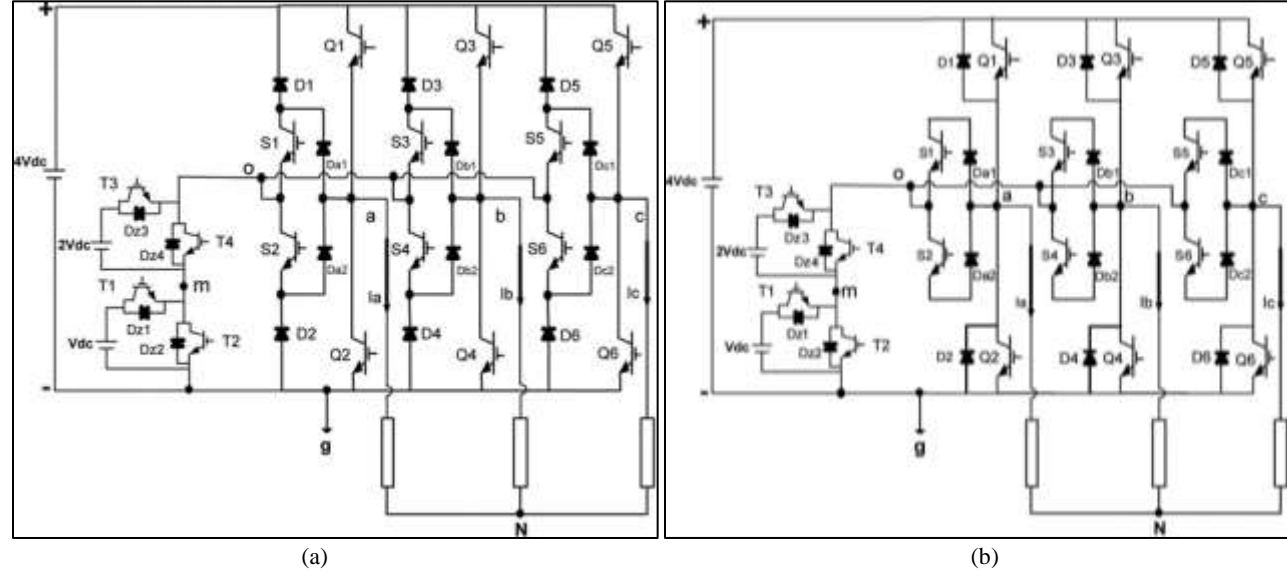


Fig. 1: Circuit Diagram of the Proposed Three-Phase Five-Level Multi-Level Inverter

A dc supply voltage Vdc of the first cell is added, if T1 (switch) is turned ON leading to Vmg = +Vdc, where Vmg means the voltage at node (m) with respect to inverter ground (g) or by-passed if T2 (switch) is turned ON leading to Vmg = 0.

Likewise, the dc supply voltage 2Vdc of the second cell is added when switch T3 is turned ON resulting in Vom = +2Vdc, where Vom is the voltage at mid-point (o) with respect to node (m) or bypassed when switch T4 is turned ON resulting in Vom = 0. The peak voltage rating of the switches of the conventional two-level bridge (Q1–Q6) is 4Vd c whereas the bidirectional switches (S1–S6) have a peak voltage rating of 3Vdc. In CHB cells, the peak voltage rating of second cell switches (T3 and T4) is 2Vd c while the peak voltage rating of T1 and T2 in case of first cell is Vdc. By considering phase a, the operating status of the switches and the inverter line-to-ground voltage Vag are given in Table 1.

 $Table - 1 \\ Switching State Sa and Inverter Line-to-Ground Voltage V_{ag}$

Sa	Q1	S1	S2	Q2	Tl	T2	T3	T4	Vag
4	on	off	off	off	on	off	on	off	+4Vdc
3	off	on	on	off	on	off	on	off	+3Vdc
2	off	on	on	off	off	on	on	off	+2Vdc
1	off	on	on	off	on	off	off	on	+Vdc
0	off	off	off	on	on	off	off	on	0

It is easier to express the inverter line-to-ground voltages V_{ag} , V_{bg} , and V_{cg} in terms of their switching states Sa, Sb, and Sc as

$$\begin{bmatrix} V_{ag} \\ V_{bg} \\ V_{cg} \end{bmatrix} = \frac{4V_{dc}}{N-1} * \begin{bmatrix} S_a \\ S_b \\ S_c \end{bmatrix}$$
 (1)

where N = 5 is the maximum number of voltage levels.

The balanced load voltages can be attained if the proposed inverter operates on the switching states represented in Table 2. Within a cycle of the output waveform, the inverter may have 24 different modes. According to Table 2, it can be observed that the bi-directional switches operate in 18 modes. For each mode, there is no more than one bi-directional switch in on-state. Because of which the load current commutates over one switch and one diode, the load current Ib will flow in S3 and Db1 or S4 and Db2). Since some insulated-gate bipolar transistors (IGBTs) share the same switching gate signals, the proposed topology significantly contributed in dropping the utilized gate driver circuits and system complexity. The inverter line-to-line voltage waveforms Vab, Vbc, and Vca with corresponding switching gate signals are depicted in Fig. 2

$$\begin{bmatrix} V_{ab} \\ V_{bc} \\ V_{ca} \end{bmatrix} = \begin{bmatrix} 1 & -1 & 0 \\ 0 & 1 & -1 \\ -1 & 0 & 1 \end{bmatrix} * \begin{bmatrix} V_{ag} \\ V_{bg} \\ V_{cg} \end{bmatrix}$$

$$(2)$$

The inverter line-to-neutral voltages VaN, VbN, and VcN may be expressed as

$$\begin{bmatrix} V_{aN} \\ V_{bN} \\ V_{cN} \end{bmatrix} = \frac{1}{3} \begin{bmatrix} 2 & -1 & -1 \\ -1 & 2 & -1 \\ -1 & -1 & 2 \end{bmatrix} * \begin{bmatrix} V_{ag} \\ V_{bg} \\ V_{cg} \end{bmatrix}$$
(3)

It is useful to recognize that the inverter voltages at terminals a, b, and c with respect to the midpoint (o) are given by

$$\begin{bmatrix} V_{ao} \\ V_{bo} \\ V_{co} \end{bmatrix} = \begin{bmatrix} V_{ag} \\ V_{bg} \\ V_{cg} \end{bmatrix} - \begin{bmatrix} V_{og} \\ V_{og} \\ V_{og} \end{bmatrix}$$

$$(4)$$

where Vog is the voltage at midpoint (o) with respect to ground (g). Vog routinely fluctuates among three different voltage values Vdc, 2Vdc, and 3Vdc as follows:

$$V_{og} = \begin{cases} V_{dc}, & \text{if Sa} + \text{Sb} + \text{Sc} \leq 5\\ 2V_{dc} & \text{if Sa} + \text{Sb} + \text{Sc} = 6\\ 3V_{dc} & \text{if Sa} + \text{Sb} + \text{Sc} \geq 7 \end{cases}$$

The simulated voltage waveforms of Vag, Vog, Vao, and VaN based on (1)–(5) are shown in Fig. 3 where, for instance, 13 Table - 2

Switching States Sequence of the Proposed Inverter within One Cycle

Sa Sb Sc	Period T[s]	ON switches Leg a	ON switches Leg b	ON switches Leg c	ON switches cascaded half-bridge	Vag [V]	Vbg [V]	Vcg [V]
400	tl	Q1	Q4	Q6	T1,T4	4Vdc	0	0
410	12	Q1	\$3, \$4	Q6	T1,T4	4Vdc	Vde	0
420	t3	Q1	\$3, \$4	Q6	T2,T3	4Vdc	2Vdc	0
430	14	Q1	\$3, \$4	Q6	T1,T3	4Vdc	3Vdc	0
440	15	Q1	Q3	Q6	T1.T3	4Vdc	4Vdc	0
340	16	\$1, \$2	Q3	Q6	T1,T3	3Vdc	4Vdc	0
240	17	S1, S2	Q3	Q6	T2,T3	2Vdc	4Vdc	0
140	18	51, S2	Q3	Q6	T1,T4	Vdc	4Vdc	0
040	.19	Q2	Q3	Q6	T1,T4	0	4Vdc	0
041	110	Q2	Q3	S5, S6	T1,T4	. 0	4Vdc	Vdc
042	111	Q2	Q3	S5, S6	T2,T3	0	4Vdc	2Vdc
043	t12	Q2	Q3	S5, S6	T1,T3	0	4Vdc	3Vdc
044	113	Q2	Q3	Q5	T1,T3	0	4Vdc	4Vde
034	114	O2	S3, S4	Q5	T1,T3	0	3Vdc	4Vdc
024	115	Q2	S3, S4	Q5	T2,T3	0	2Vdc	4Vdc
014	116	Q2	S3, S4	Q5	T1,T4	0	Vdc	4Vdc
004:	t17	Q2	Q4	Q5	T1,T4	0	0	4Vdc
104	118	S1, S2	Q4	Q5	T1.T4	Vdc	0	4Vde
204	119	S1, S2	Q4	Q5	T2,T3	2Vdc	0	4Vdc
304	t20	S1, S2	Q4	Q5	T1,T3	3Vdc	0	4Vdc
404	121	Q1	.04	Q5	T1,T3	4Vdc	0	4Vdc
403	122	Q1	Q4	S5, S6	T1,T3	4Vdc	0	3Vdc
402	123	01	Q4	S5, S6	T2,T3	4Vdc	0	2Vdc
401	124	01	04	S5, S6	TLT4	4Vdc	0	Vde

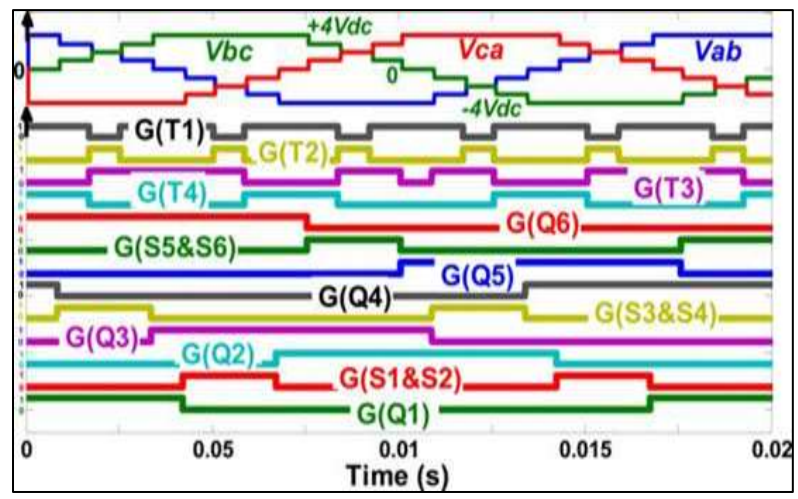


Fig. 2: Simulated waveforms of Vab, Vbc, and Vca with corresponding switching gate signals for the proposed inverter at fundamental frequency f = 50 Hz

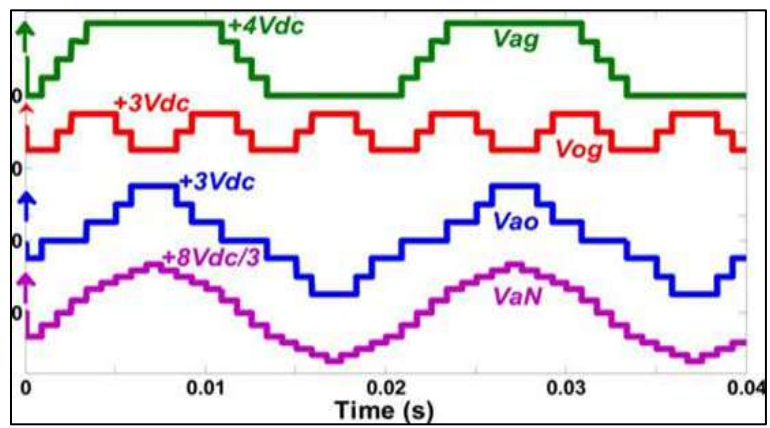


Fig. 3: Simulated waveforms of Vag, Vog, Vao, and Va N for the proposed inverter f = 50 Hz

The sequent voltage steps are seen in VaN waveform as follows: +8Vd c/3, +7Vd c/3, +6Vd c/3, +5Vd c/3, +4Vd c/3, +2Vd c/3, -2Vd c/3, -4Vd c/3, -5Vd c/3, -6V dc/3, -7Vd c/3, and -8Vd c/3. It is worth noting that all simulated waveforms are obtained at t1 =t2 = $\cdot \cdot \cdot$ = t2 4 = 0.02/24 s. In order to plot the space vector diagram of the proposed inverter in a stationary d–q reference frame, the following equations can be used to derive d and q voltage components for all inverter vectors:

$$V_{q} = \frac{4V_{dc}}{3(N-1)} (2S_{a} - S_{b} - S_{c})$$
 (6)

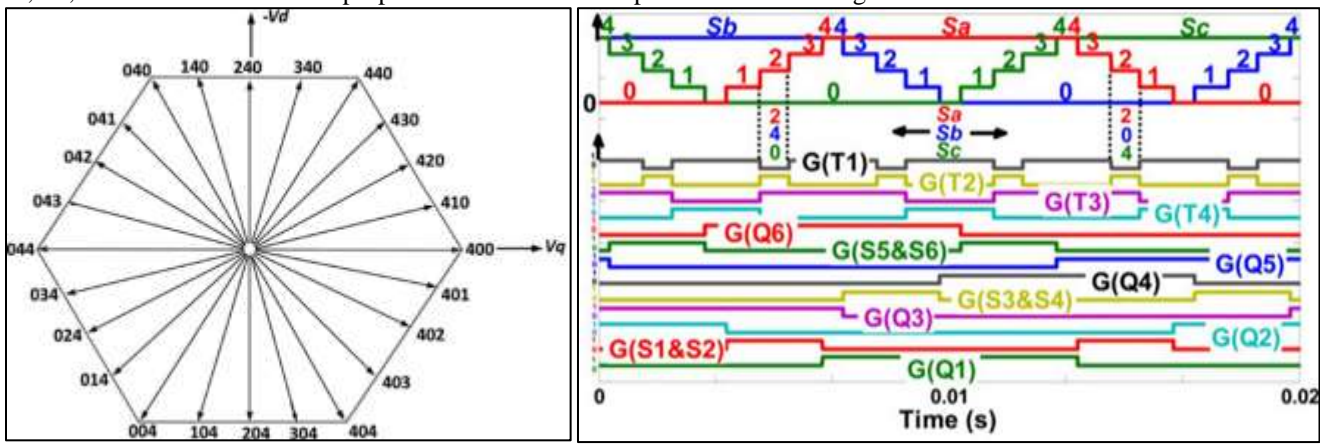
$$V_{d} = \frac{4V_{dc}}{\sqrt{3}(N-1)} (S_{c} - S_{b})$$
 (7)

$$V = V_q - jV_d \tag{8}$$

For all switching states presented in Table II, Fig. 4 shows the space vector diagram for the proposed topology.

III. SWITCHING ALGORITHM

For the proposed inverter, we can simply implement the staircase modulation. The most common modulation technique used to control the fundamental output voltage as well as to eliminate the unwanted harmonic components from the output waveforms is Staircase modulation with selective harmonic. The Newton–Raphson method is normally used to find out the solutions to (N–1) non-linear transcendental equations. The problematic calculations and the need of high performance controller for the real time applications are the main disadvantages of such method. Hence, an alternative method is proposed to produce the inverter's switching gate signals. It is very easy to control the proposed inverter and achieve the required output voltage waveforms in terms of Sa, Sb, and Sc. The basis of the proposed method can be explained as succeeding:



Or a given value of modulation index Ma and within a full cycle of the operation of the proposed inverter, the switching states Sa, Sb, and Sc are determined instantly. The on-time calculations of Sa, Sb, and Sc directly depend on the instantaneous values of the inverter line-to-ground voltages. It is very well known that the reference values of Vag, Vbg, and Vcg are normally given by

$$\begin{bmatrix} V_{ag_ref} \\ V_{bg_ref} \\ V_{cg_ref} \end{bmatrix} = \frac{M_a * 4V_{dc}}{2} * \begin{bmatrix} \cos(wt) \\ \cos(wt - \frac{2\pi}{3}) \\ \cos(wt + \frac{2\pi}{3}) \end{bmatrix} + \frac{4V_{dc}}{2} * \begin{bmatrix} 1 \\ 1 \\ 1 \end{bmatrix}$$

where wt is the electrical angle. Or

$$\begin{bmatrix} V_{ag_ref} \\ V_{bg_ref} \\ V_{cg_ref} \end{bmatrix} = \frac{M_a * 4V_{dc}}{2} * \begin{bmatrix} \cos(wt) \\ \cos(wt - \frac{2\pi}{3}) \\ \cos(wt + \frac{2\pi}{3}) \end{bmatrix} + \frac{4V_{dc}}{2} * \left[1 - \frac{M_a}{6} \cos(3wt) \right] * \begin{bmatrix} 1 \\ 1 \\ 1 \end{bmatrix}$$
(10)

From (10), it can be observed that the third harmonic component is summed to the three-line-to-ground voltages. The third harmonic injection may rise the inverter fundamental voltage without causing over modulation. As a result, Ma can reach to 1.15 and Sa, Sb, and Sc can be simply determined by integerzing the reference line-to-ground voltages as

$$\begin{bmatrix} S_{a} \\ S_{b} \\ S_{c} \end{bmatrix} = \text{int } eger \left(\frac{N-1}{4V_{dc}} * \begin{bmatrix} V_{ag_ref} \\ V_{bg_ref} \\ V_{cg_ref} \end{bmatrix} \right)$$
(11)

The proposed modulation method is compared with the Stair case modulation with the selective harmonic method. The proposed modulation features needs less time and have simple calculations. The inverter's operating switching states Sa, Sb, & Sc and the corresponding switching gate signals based on the proposed modulation method are shown in Fig. 5.Fig. 5. Inverter's operating switching states Sa, Sb, & Sc with corresponding switching gate signals based on the proposed modulation method.

Table 3
Switching State Sa1 & Inverter Line-To-Ground Voltage Vag AT Ma < 0.9 (LEG a)

Sal	QI	SI	S2	Q2	TI	T2	<i>T3</i>	T4	Vag
2	On	off	off	off	off	On	On	off	+4 <i>Vdc</i>
1	off	On	On	off	off	On	On	off	+2Vdc
0	off	off	off	On	off	On	On	off	0

It is clear that the switching gate signals are generated within 24 different modes starting from (044) to (034). Since the proposed converter has been designed in order to achieve 5 voltage levels, the modulation index must be within range $0.9 \le Ma \le 1.15$. For modulation index Ma < 0.9, only two dc voltage supplies 4Vdc and 2Vdc are employed and the behavior of the proposed inverter becomes similar to the three-level multi-level inverter. Using (9)–(11) and substituting N = 3, the inverter's operating switching states Sa, Sb, and Sc at Ma < 0.9 can be defined. The principle of operation of the proposed inverter at Ma <0.9 is illustrated in Table 3. Fig. 6(a) and Fig. 6(b) shows the inverter line-to-line voltage waveforms at 5 different modulation indices including the over modulation operation Ma = 0.8, 0.9, 1.05, 1.15, and 1.3.

IV. EXTENDED STRUCTURE

It is noticeable that there is possibility to reach an output voltage with higher number of steps in the proposed multilevel inverter by extending the CHB circuit. Such extending can be done by adding more half-bridge cells connected in series as shown in Fig. 7(a) and (b). In order to achieve the desired number of voltage levels, three methods can be followed to determine the magnitudes of utilized dc voltage supplies.

1) All cells have an equal dc supply in magnitude.

$$V_{dc1} = V_{dc2} = \dots = V_{dcn} = V_{dc}$$
 (12)

Then, the magnitude of fixed dc supply can be chosen as

$$V_{fix} = (N-1)V_{dc} = (1+n)V_{dc}$$
(13)

where n is the number of utilized cells. The maximum number of voltage steps is related to the number of utilized cells by

$$N = n + 2 \tag{14}$$

The number of operation modes that makes the switching states sequence achieves the required output voltage waveform can be expressed as

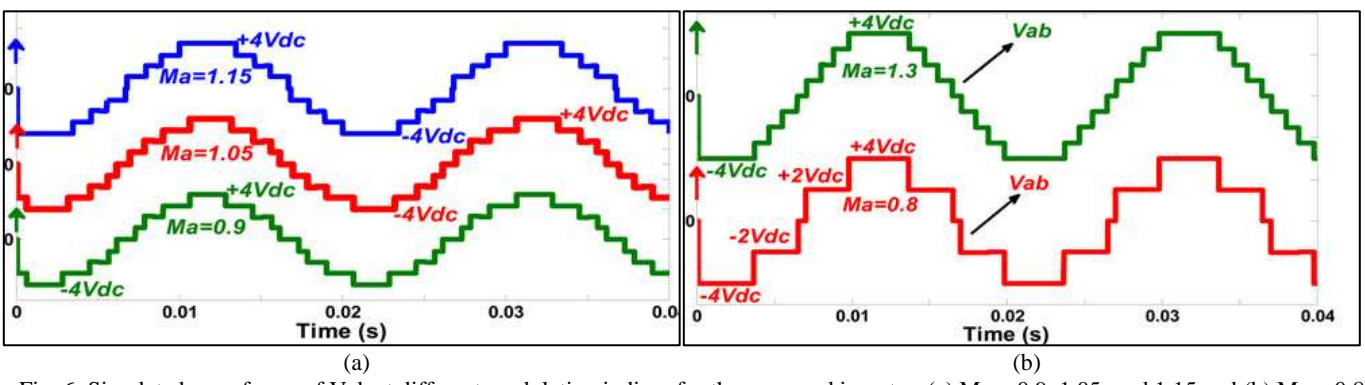


Fig. 6: Simulated waveforms of Vab at different modulation indices for the proposed inverter: (a) Ma = 0.9, 1.05, and 1.15 and (b) Ma = 0.8 and 1.3

$$M = 6 (N - 1)$$
 (15)

2) The magnitude of dc voltage supply used in each and every cell in a particular inverter is obtained as follows:

$$V_{dc1} = V_{dc} \tag{16}$$

$$V_{dc2} = 2V_{dc} \tag{17}$$

$$V_{dcn} = nV_{dc} \tag{18}$$

$$V_{fix} = (N-1)V_{dc} = \left[1 + \frac{n(n+1)}{2}\right]V_{dc}$$
 (19)

$$N = 2 + \frac{n(n+1)}{2} \tag{20}$$

$$M = 6 (N - 1)$$
 (21)

3) By making a binary (power of 2) relationship between the dc supplies of the CHB structure as follows:

$$V_{dc1} = 2^{(0)}(V_{dc}) (22)$$

$$V_{dc2} = 2^{(1)}(V_{dc}) (23)$$

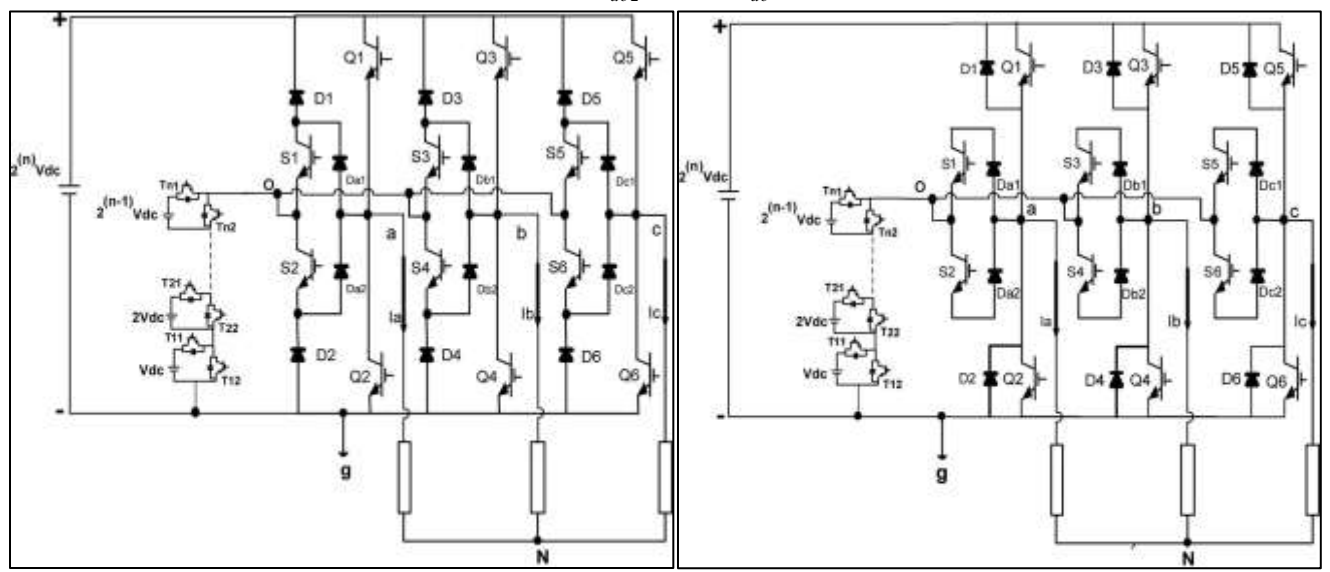


Fig. 7: Circuit Diagram of the Proposed Three-Phase N-Level Multi-Level Inverter (Third Method)

$$V_{dcn} = 2^{(n-1)}(V_{dc}) (24)$$

$$V_{fix} = (N-1)V_{dc} = \left[1 + \sum_{j=1}^{n} 2^{j-1}\right]V_{dc} = (2^{n})V_{dc}$$
 (25)

$$N = 1 + 2^n \tag{26}$$

$$M = 6(N-1) \tag{27}$$

Table 4 illustrates some characteristics of the proposed methods.

Table - 4

Comparison of the Maximum Number of Voltage Levels with the Required Value of DC Voltage Supplies among the Proposed Methods

No of Cells	First			Second			Third			
No of Cells	Method				Method			Method		
N	N	M	Vfix	N	M	Vfix	N	М	Vfix	
2	4	18	3Vdc	5	24	4Vdc	5	24	4Vdc	
3	5	24	4Vdc	8	42	7Vdc	9	48	8Vdc	
4	6	30	5Vdc	12	66	11Vdc	17	96	16Vdc	
5	7	36	6Vdc	17	96	16Vdc	33	192	32Vdc	
6	8	42	7Vdc	23	132	22Vdc	65	384	64Vdc	

Based upon the comparison carried among the various proposed methods, some observations are given below.

- 1) The first method as compared to the second and third methods, has a high modularity degree because of the symmetric structure of CHB makes use of equal dc voltage supplies. This method helps the proposed inverter to reach the maximum number of voltage levels (4, 5, 6, 7, 8, . . ., N).
- 2) Since the second and third methods use the asymmetrical structure of CHB, the proposed inverter can reach the necessary output voltage and the maximum number of voltage levels such as 5, 8, 9, 12, 17,... with less number of dc supply voltages and power electronic components.

V. COMPARISON STUDY

In order to investigate the capability of the suggested topology, the proposed inverter is compared with different types of multilevel inverters such as Neutral Point Clamped (NPC), Flying Capacitor (FC), and the Cascaded H-Bridge (CHB). It is obvious that the suggested three-phase N-level multi-level inverter can considerably reduce the required number of power electronic components. For the same number of output voltage levels ($N \ge 4$), Table 5 describes the required number of dc voltage supplies, control signals, switches, clamping diodes, and balancing capacitors of the proposed N-level inverter compared with the three existing inverters Neutral Point Clamped (NPC), Flying Capacitor (FC), and the Cascaded H-Bridge (CHB). As shown in Fig. 8, it can be observed that nearly more than two-third of number of switches can be counted out as N increases. For example, at the same number of voltage levels N = 17, and when compared with the existing multi-level inverters which require 96 switches, the required number of switches for the proposed inverter is comparatively less, since it requires 42 switches based on the first method, 22 switches based on the second method, and 20 switches based on the third method. On the other hand, it is well-known that the voltage and current ratings of the power electronic components have an effect on the cost and realization of the multi-level inverter. Assuming that all power components have an equal current rating which is the rated current of the load (IL), the voltage ratings of these components depend on the magnitude of dc supply voltage, voltage stress, and structure of the inverter. Considering that all inverters have the same input dc link which equals (N-1) Vdc, Table 6 illustrates the rating requirements for the proposed inverter when compared with the rating requirements for the existing inverters. It is observed that the inverter employs switching devices with high voltage rating. That results in high cost per-switch. Since the topology is introduced with reduced number of switches, gate driver circuit, diodes and no clamping capacitors are employed, the semiconductor devices expenses are considerably recovered.

VI. POWER CONVERSION EFFICIENCY & TOTAL HARMONIC DISTORTION (THD %)

In order to regulate the efficiency of the proposed inverter, it is necessary to determine the value of conduction and switching power losses generated by the power electronics components. Basically, the main losses in semiconductor components such as IGBTs and diodes are categorized into two groups: Switching loss (Psw) & conduction loss (Pcon) as follows:

$$P_{sw_IGBT} = \frac{1}{T} \int_{0}^{T} E_{on}(t) dt + \frac{1}{T} \int_{0}^{T} E_{off}(t) dt$$
 (28)

$$P_{sw_diode} = \frac{1}{T} \int_{0}^{T} E_{rr}(t) dt$$
 (29)

Where Eon(t) is a turn-on loss and E off (t) is a turn-off loss. Switching losses Eon(t) and Eoff (t) are experienced during the ON and OFF states, respectively. While Err(t) is the reverse recovery loss of the diode, the majority of switching loss, which is experienced when the diode is in OFF state.

$$P_{con_IGBT} = \frac{1}{T} \int_{0}^{T} V_{on_IGBT} i(t) dt$$
(30)

$$P_{con_Diode} = \frac{1}{T} \int_{0}^{T} V_{on_diode} i(t) dt$$
(31)

Conduction power losses of IGBT and diode are approximated based on their forward voltage drops Von IGBT, Von diode, and the instantaneous current i(t) flowing through IGBT or diode. The total losses Pt are expressed as follows:

$$P_{t} = P_{con} + P_{sw} \tag{32}$$

Once the total semiconductors losses Pt in the introduced inverter are defined, the relative inverter efficiency is determined based on the following expression:

$$n\% = \frac{P_{out}}{P_t + P_{out}} \times 100 \tag{33}$$

The probable current directions with corresponding conducting devices in phase are given in Table 7. A MATLAB/Simulink model of the proposed inverter shown in Fig. 1 has been developed to study the conduction and switching power losses. The proposed inverter is designed to deliver output power (Pout = $1.9 \, \text{kW}$). A three-phase series resistive—inductive (23Ω , 3 mH/Phase) in star connection is used as load. The multi- Level dc link is determined as Vdc = $75 \, \text{V}$, 2Vdc = $150 \, \text{V}$, and Vfix = $4 \, \text{Vdc} = 300 \, \text{V}$ and the proposed staircase modulation technique at Ma = 1 is used to generate the appropriate switching gate signals. Three different types of power electronic components are selected to build the prototype of the proposed inverter power circuit as following: IGBT (HGTG20N60B3D) 600V/40A for the two-level bridge and CHB switches, IGBT (IRG4BC40W) 600V/20A for bi-directional switches, and Diode (RHRP1540) 400V/15A for embedded diodes in bi-directional switches and freewheeling diodes. The data sheets of the utilized semiconductor components can be easily accessed to obtain their characteristic curves.

Table - 5
Comparison of the Proposed N-Level Inverter with the Existing Inverters

G			•	PROPOSED METHODS				
Converter Type	NPC	FC	СНВ	1ST	2ND	3RD		
Switches	6(N-1)	6(N-1)	6(N-1)	2(N-1)+10	$\sqrt{8N-15}+11$	$2Log_{2}(N-1)+12$		
Gate Drivers	6(N-1)	6(N-1)	6(N-1)	2(N-1)+7	$\sqrt{8N-15}+8$	$2Log_{2}(N-1)+9$		
Diodes	6(N-1)	6(N-1)	6(N-1)	2(N-1)+10	$\sqrt{8N-15} + 11$	$2Log_{2}(N-1)+12$		
Clamping Diodes	6(N-2)	0	0	0	0	0		
DC Supplies	(N-1)	(N-1)	3(N-1)/2	(N-1)	$1 + \left[(\sqrt{8N - 15} - 1)/2 \right]$	$1 + Log_2(N-1)$		
Clamping Capacitors	0	3(N-2)	0	0	0	0		
Control Signals	6(N-1)	6(N-1)	6(N-1)	2(N-1)+7	$\sqrt{8N-15}+8$	$2Log_{2}(N-1)+9$		

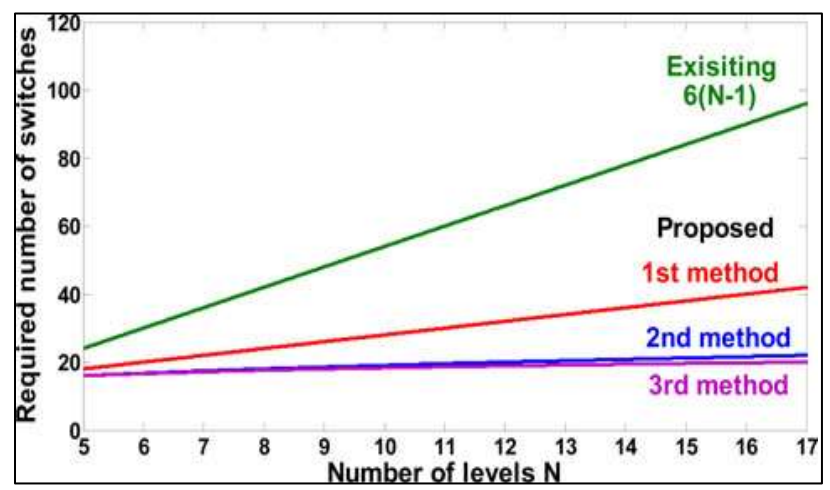


Fig. 8: Comparison of Required Number of Switches among Existing Inverters and the Proposed Topology

The mathematical models obtained for HGTG20N60B3D 600 V/40 A are given by

$$V_{on_IGBT\ 1} = 1.418 e^{0.016t(t)}$$
(34)

$$E_{on_IBGBT\ 1} = (201.6e^{0.04418t(t)} - 291.6e^{-0.1265t(t)} \times 10^{-6}$$
(35)

$$E_{off_IGBT\ 1} = (323.3e^{0.05125t(t)} \times 10^{-6}$$
(36)

To simplify the losses calculation, a curve-fitting tool of MATLAB is used to approximate these curves by exponential equations [35]. While the mathematical models obtained for IRG4BC40W 600V/20A are given by

$$V_{on_IGBT\ 2} = 1.555 e^{0.0085371t(t)}$$
(37)

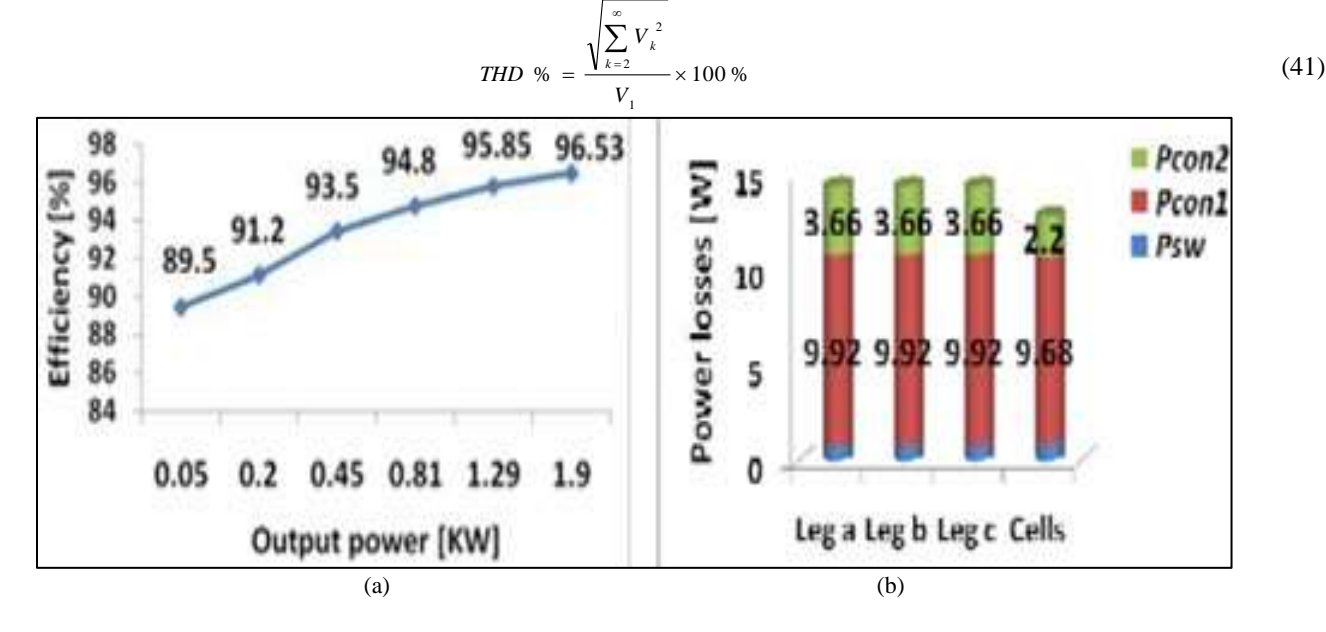
$$E_{sw_IGBT\ 2} = (0.340 e^{0.04472t(t)}) \times 10^{-3}$$
(38)

And finally, the mathematical models obtained for RHRP1540 400V/15A are given by

$$V_{on_diode} = 1.325 e^{0.006424t(t)} - 0.8571 e^{0.07183t(t)}$$
(39)

$$E_{rr\ diode} = (15.7e^{-0.002733t(t)} + 2.74e^{-0.1413t(t)} - 3.162e^{-0.05923t(t)} - 8e^{-0.09452}) \times 10^{-6}$$
(40)

Hence, the conduction and switching power losses for the inverter switches and diodes can be estimated by substituting equations (34)–(40) into equations (28)–(33). When the input voltage is raised in small steps, the efficiency of the proposed inverter is estimated. Fig. 9(a) represents the estimated value of efficiency over a wide range of the output power. It is clear that the inverter's efficiency is directly proportional to the output power and reaches its optimized value of 96.53% at 1.9 kW. It is a result of more power being effectively transferred with respect to the power losses. Moreover, the distribution of power losses among the inverter's legs and the CHB cells are shown in Fig. 9(b). The distribution of power losses is attained during the operation of the proposed inverter to deliver Pout = 1.287 kW at step voltage Vdc = 62.5 V, 2Vdc = 125 V, and Vfix = 4Vdc = 250 V. The generated power losses by the legs a, b, and c are almost equal and slightly higher than those generated by CHB cells. According to Fig. 9(b), 53.3% of the total value of power loss is experienced in the conventional two-level bridge, since 3×9.92 W in term of conduction power losses is generated by Q1-Q6. It is absolutely due to fact that the conduction power loss is directly proportional to the switching conduction time and the value of conducting current (for instance, O1 and O2 conduct the load current in 18 modes). Insignificantly conduction power losses are generated by the free whiling diodes (D1–D6). Further measurements show that 9.68 + 2.2 W is the estimated value of the conduction power losses generated by CHB's switches and diodes. It is almost 21.3% of total power loss. The higher conduction power loss is experienced in T3 followed by T1, T4, and T2. The three bi-directional switches contribute to 19.6% of the total power loss as 3×3.66 W is the projected value of conduction power loss generated by S1–S6 and Da1–Dc2. Finally, it can be observed that a switching loss which is almost negligible is generated since the fundamental frequency is implemented. Additionally in order to assess the performance of the proposed inverter comparing with other types of the multilevel inverter, a five-level NPC multi-level inverter built by IRG4BC40W 600V/20A and RHRP1540 400V/15A semiconductor component types has been modeled and operated under the same conditions to the proposed inverter. The projected value of efficiency and power losses distribution of the NPC multi-level inverter are shown in Fig. 9(c) and (d). By comparing the proposed inverter's efficiency with the five-level NPC multi-level inverter's efficiency shows that the proposed inverter has a higher efficiency since the maximum estimated efficiency of the NPC multilevel inverter is 93.85%. The lower Pt generated by the proposed inverter comparing with Pt generated by the five-level NPC multilevel inverter is a result of the low conduction power losses and reduced number of power components. A lower voltage stress leads to a lower switching power loss. However, the more the switching devices, the higher the conduction power losses. At the same operating point Pout ≈ 1.287 kW and compared with the estimated value of Pt proposed = $3\times14.4+12.78\approx55.9$ W generated by the proposed inverter, the estimated value of Pt generated by the NPC multilevel inverter is two times higher. It is nearly Pt NPC = $3 \times 37.5 \approx 112.5$ W. Moreover, the proposed inverter has been tested under different modulation indices (Ma = 0.9, 1, and 1.15). THD% of the output voltage can be calculated by



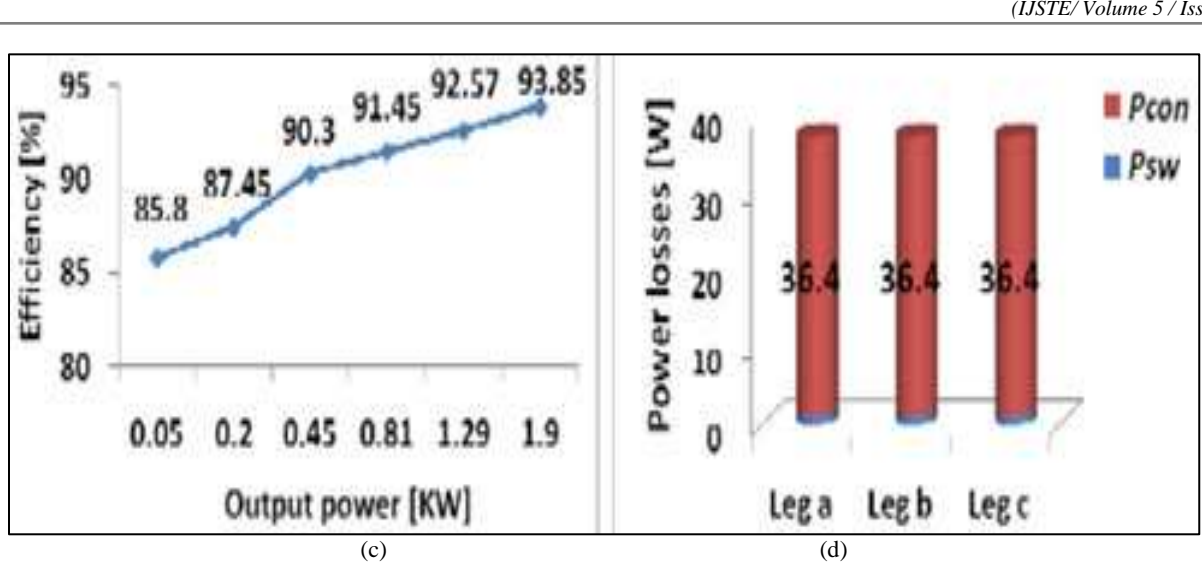


Fig. 9: Power loss and efficiency comparison. For the proposed inverter: (a) output power versus efficiency, (b) Pcon and Psw distribution among legs a, b, c, and CHB cells for Ma = 1 and Pout = 1.287 kW. For the NPC inverter: (c) output power versus efficiency and (d) Pcon and Psw distribution among legs a, b, and c for Ma = 1 and Pout = 1.285 kW

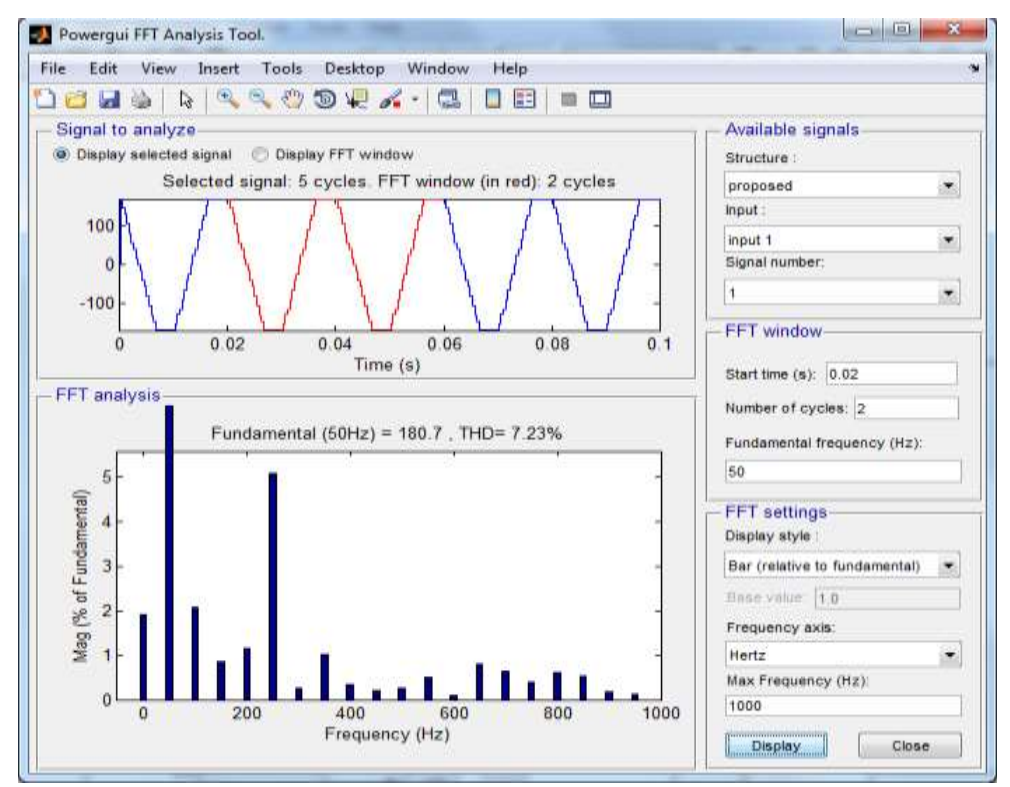


Fig. 10: NPC, FC, CHB, & Proposed Inverter: Line-To-Line Voltage THD% versus Ma

Table - 6
Proposed & the Existing Topologies Rating Requirements per Level N

Proposed Inventor	Main Bridge	Bidirectional Switches	Cascaded Half-Bridge Switches Tl1 to Tn2			Converter Type	NPC	FC	СНВ
Proposed Inverter	Q1-Q6 D1a-D2c	S1 to S6 D1 to D6	1 st Method	2 nd Method	3 rd Method	Switches Voltage Rating	V_{dc}	V_{dc}	V_{dc}
Component Voltage rating	(N-1) V _{dc}	(M 2)V.	W	17	$2^{(n-1)} V_{dc}$	Clamping Diode Voltage Rating	V_{dc}	0	0
		$(N-2)V_{dc}$	V_{dc}	$n V_{dc}$		Clamping Diode Voltage Rating	0	V_{dc}	0
Active Components current	IL	IL	IL	IL	IL	Active Component Current	IL	IL	IL

Table - 7
Conducting Devices of the Proposed Inverter Phase a

Current	Conducting Devices Phase a. Fig. 1(a)	Vag	Conducting Devices Phase a. Fig. 1(b)	Vag
	Q1	+4Vdc	Q1	+4Vdc
	T1, T3, S2, Da2	+3Vdc	T1, T3, S2, Da2	+3Vdc
Ia > 0	Dz2, T3, S2, Da2	+2Vdc	Dz2, T3, S2, Da2	+2Vdc
	T1, Dz4, S2, Da2	+Vdc	T1, Dz4, S2, Da2	+Vdc
	D2, Da2	0	D2	0
	D1, Da1	+4Vdc	D1	+4Vdc
	Dz1, Dz3, S1, Da1	+3Vdc	Dz1, Dz3, S1, Da1	+3Vdc
Ia < 0	T2, Dz3, S1, Da1	+2Vdc	T2, Dz3, S1, Da1	+2Vdc
	Dz1, T4, S1, Da1	+Vdc	Dz1, T4, S1, Da1	+Vdc
	O2	0	O2	0

Where V1 and Vk are the fundamental component and harmonic order, respectively. NPC, FC, and CHB multi-level inverters have been tested under the same operating conditions. The aim of this test is to compare the proposed inverter with the existing inverters in term of THD%. Fig. 10 shows THD% of the line-to-line voltage for all inverters within specific range of modulation indices [0.9–1.15]. It can be seen that the THD% of all inverters are slightly different. The measured values of THD% for the proposed inverter are within a range of 8.4–13.25%. As a result, the proposed inverter basically adds the attractive aspects of the traditional two-level inverter such as less power electronic components, simple working principle, and minimum conduction power loss to the main advantages of the multi-level inverter such as low THD% and high output voltage quality.

VII. EXPERIMENTAL RESULTS

To ensure the feasibility of the proposed topology, the inverter concept was implemented and its prototype has been manufactured. During the hardware implementation, the inverter shown in Fig. 1 was tested under Vdc = 22.5 V in the first cell and 2Vdc = 45 V in the second cell.

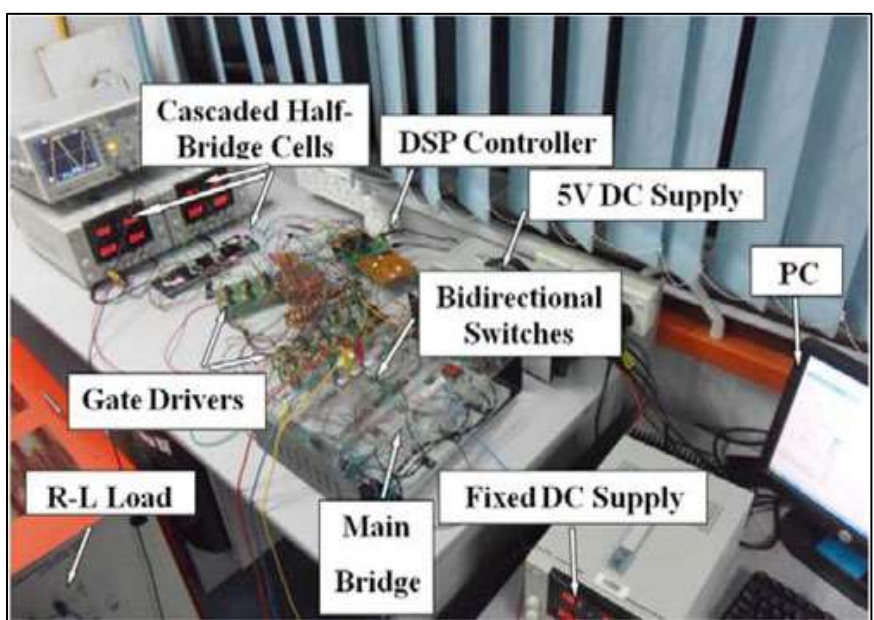


Fig. 11: Prototype of the Proposed Multilevel Inverter

Table - 8
Specifications of the Semiconductors

Six-Switched Bridge IGBTs (Q1-Q6)	HGTG20N60B3D,40A,600V
Half-Bridge Cells IGBTs (T1-T4)	HGTG20N60B3D,40A,600V
Bi-directional Switches IGBTs (S1-S6)	IRG4BC40W, 20A, 600V
Diodes	RHRP1540,15A,400V

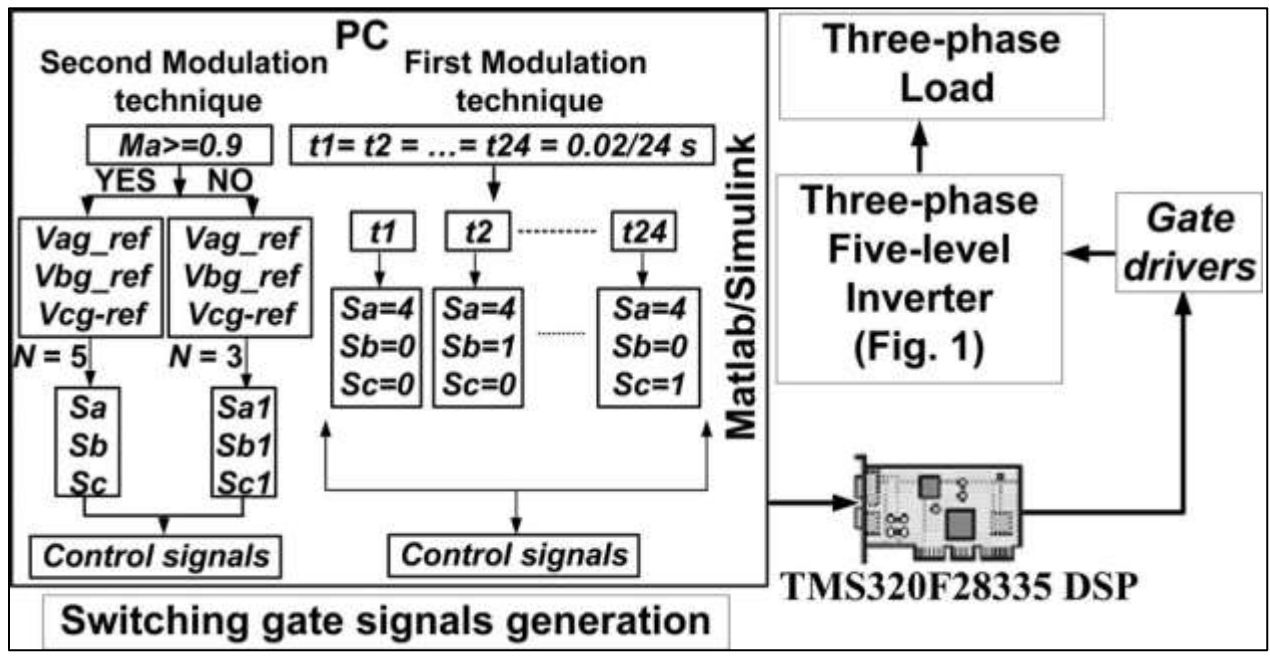


Fig. 12: Control Block Diagram

The magnitude of the fixed dc supply is determined as V fix = 4V dc = 90 V. A star connected fixed three-phase series resistive inductive load (23Ω-3mH/Phase) was used. In order to generate the appropriate switching gate signals, a DSP controller was used. The fundamental frequency f = 50 Hz staircase modulation technique was employed. In Fig. 11, the prototype of the proposed inverter is shown. It consists of the following components: personal computer, TMS320F28335 DSP controller, conventional sixswitch bridge, fixed dc supply voltage, 13 gate drivers, three bi-directional switches, two half-bridge cells powered by 5 V dc supply, and fixed three-phase (R - L) load. The type of semiconductors used for the power circuit is provided in Table 8. Two modulation techniques are implemented to operate the proposed inverter as illustrated in the control block diagram (see Fig. 12). In the 1st modulation technique, the generation principle of the switching gate signals depends on time duration presented in Table 2, where the time duration of a cycle of the output waveform (t = 1/50 = 0.02 s) is divided into 24 equal time periods: $t1=t2=\cdots$ t24 = 0.02/24s. During each period, the proposed inverter' switches are turned ON/OFF following the switching sequence illustrated in Table 2. In Fig. 13(a) and (b), there is an illustration of the switching gate signals of the four switches (Q1, S1, S2, and Q2) in leg of the main bridge and the four switches (T1, T2, T3, and T4) in the CHB circuit. The shapes of switching gate signals of switches in legs b and c are similar to those shown in Fig. 13(a) but they are shifted by 0.02/3 and 0.04/3 s, respectively. The operating frequencies fsw of the proposed inverter' switches can be determined by means of the number of pulses per cycle as following: Q1-Q6 of the conventional bridge are turned ON/OFF at fsw=f = 50 Hz, while the bidirectional switches (S1-S6) are turned ON/OFF at fsw = 2f = 100 Hz. fsw = 6f = 300 Hz and fsw = 4f = 200 Hz are the operating frequency of the first cell switches T1 and T2 and the second cell switches T3 and T4, respectively. Fig. 13(c) depicts the inverter line-to-ground voltages Vag, Vbg, and Vcg. It is clear that the controller manages to generate the appropriate switching gate signals that lead the inverter to output the desired waveform with five voltage steps. The inverter line-to-line voltages Vab, Vbc, and Vca waveforms with nine levels and the inverter line-to-neutral voltages VaN, VbN, and VcN waveforms with 13 levels are shown in Fig. 13(d) and (e), respectively. In Fig. 13(f), the inverter terminal voltages Vao, Vbo, and Vco reached their maximum value 3Vdc with seven voltage steps as planned. Based on shapes of Vag and Vog, Vog takes three different voltage values and it repeats itself three times within a full cycle of Vag as shown in Fig. 13(g). In Fig. 13(h), the experimental waveforms of load current and line-to-neutral voltage of phase are shown.

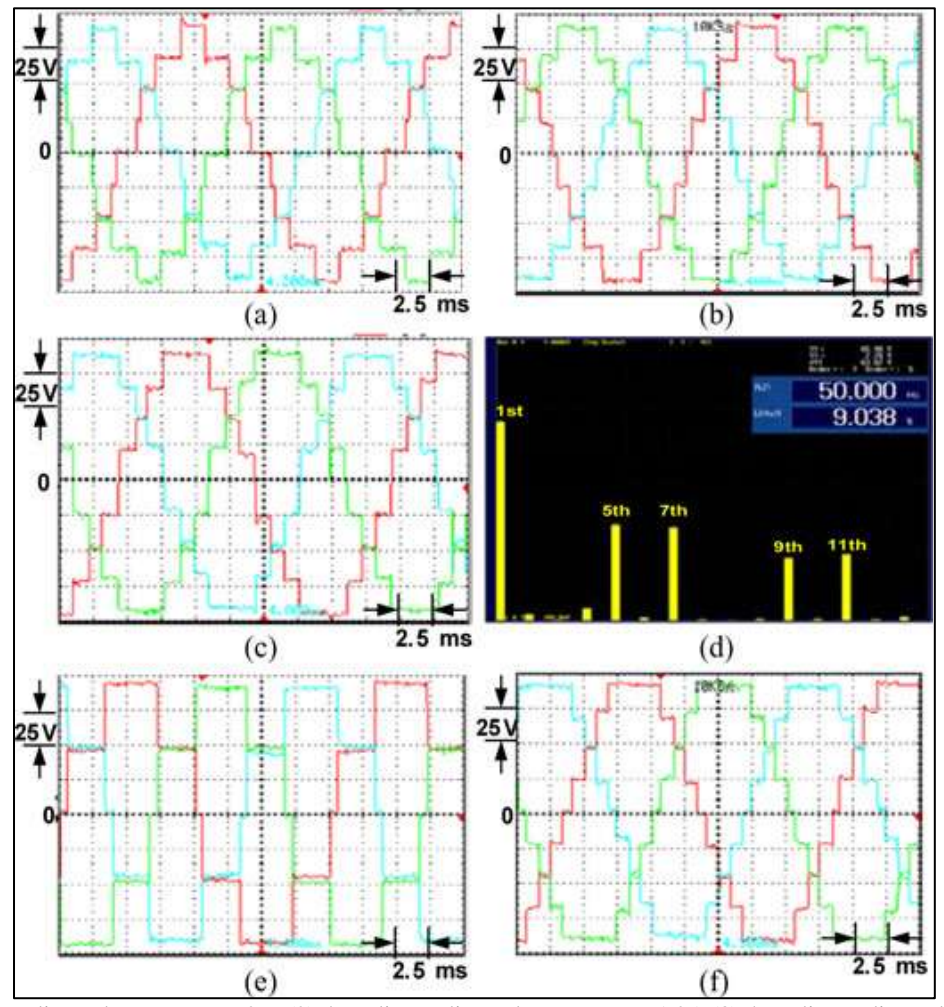


Fig. 14: (1) Three-line-to-line voltages at Ma = 0.9, (2) three-line-to-line voltages at Ma = 1.05, (3) three-line-to-line voltages at Ma = 1.15, (4) THD% at Ma = 1.15, (5) three-line-to-line voltages at Ma = 0.8, and (6) three-line-to-line voltages at Ma = 1.3

In order to investigate the performance of the proposed inverter at different modulation indices, the modulation procedure presented in Section III is executed. The proposed configuration was tested under different modulation indices Ma = 0.9, 1, and 1.15. Fig. 14(1), (2), and (3) shows the inverter balanced line-to-line voltage waveforms. These voltage waveforms are similar to those obtained through simulation in Section III. THD% and the harmonic content of the line-to-line voltage Vab at Ma = 1.15 are shown in Fig. 14(4). The graph contains the fundamental frequency component followed by 14 harmonics components. Due to the symmetry attained in the inverter output line-to-line voltage, all the even harmonic components are almost eliminated. Also, the triplen harmonic components such as 3rd, 9th, and 15th are eliminated. A lower harmonic components lead to a lower THD%. The measured THD% is found around 9.038%. The measured (rms) value of the fundamental frequency component of the line-to-line voltage waveform Vab is 63.61V. It is nearly $1.15 \times (0.612 \times 4 \text{Vdc})$ where $0.612 \times 4 \text{Vdc} = 55.08 \text{ V}$ is the maximum (rms) value of the fundamental frequency component at Ma = 1. It can be seen that the (rms) value of the fundamental frequency component shown in Fig. 14(4) is improved by 15% at low THD%. The Fig. 15. Experimental results of (a) output power versus efficiency for the proposed inverter and (b) line-to-line voltage THD% versus Ma for Vdc = 75V. The normalized value of the larger harmonic component (5th) is 3.42/63.61 = 0.053. By applying staircase modulation with selective harmonic, the present harmonic components such as 5th, 7th, and 11th can be eliminated. It is worth noting that the estimation of optimal switching angles is not the objective of this paper. Decreasing the modulation index to Ma = 0.8 results in three positive levels (0, +2Vdc, and +4Vdc) in the inverter output line-to-line voltage waveforms as shown in Fig. 14(5). Such decreasing makes the proposed configuration operates as a traditional three-level inverter. The over modulation happens when the proposed inverter is operated at Ma > 1.15. Fig. 14(6) represents the experimental voltage waveforms of the proposed inverter at Ma = 1.3. Further studies were conducted to verify the efficiency of the proposed inverter at the fixed R - L load. The efficiency took different values at different voltages supplied from the dc link as represented in Fig. 15(a). 1.9 kW of power was reached at modulation index Ma = 1. However, Vdc took the maximum value of 75 V. Since Vfix = 4Vdc and during the testing the maximum dc value was supplied from Vfix that increased upto 300 V, the inverter's efficiency can be calculated based on the measured data as follows:

$$n\% = \frac{P_{out}}{P_{in}} \times 100 \tag{42}$$

Where Pin and Pout are the inverter input and output power, respectively. The digital meter was utilized to measure Pin and Pout. The efficiency takes values around 88% under low power conditions. However, better efficiency is attained at higher power as 95.2% is the measured efficiency at 1.9 kW. By comparing the measured efficiency shown in Fig. 15(a) with the calculated efficiency shown in Fig. 9(a), it can be seen that the measured efficiency is slightly lower than calculated. It is due to supplementary loss generated by cable resistance and measurements accuracy. If this further loss is considered and added, both measured and calculated efficiencies show a close agreement. Hence, the proposed inverter is promising configuration that may serve in many applications. The variation of THD% with the modulation index for the inverter line-to-line output voltage is shown in Fig. 15(b). This demonstrates that THD% is inversely proportional to the modulation index Ma. In other words, a lower THD% in the output voltage is experienced at higher modulation index.

VIII. CONCLUSION

A new topology of the three-phase five-level (multi-level) inverter was introduced. The proposed configuration was obtained by reducing the number of power electronic components used. Thus, the proposed topology results in decrease in cost and installation area. The fundamental frequency staircase modulation topology was easily engaged and showed high flexibility and simplicity in control. Besides, the proposed configuration was extended to N-level with different methods. Furthermore, the method employed to determine the magnitudes of the dc voltage supplies was well executed. In order to validate the performance of the proposed multi-level inverter, the proposed configuration was simulated and its prototype was manufactured. The obtained simulation and hardware results met the desired output. Henceforth, subsequent work in the future may include an extension to higher level with other recommended methods. For purpose of minimizing THD%, a selective harmonic elimination pulse width modulation (PWM) technique can be also executed.

REFERENCES

- [1] J. Rodriguez et al., "Multilevel inverters: A survey of topologies, controls, and applications," IEEE Trans. Ind. Electron., vol. 49, no. 4, pp. 724–738, Aug. 2002
- L. G. Franquelo et al., "The age of multilevel converters arrives," IEEE Ind. Electron. Mag., vol. 2, no. 2, pp. 28-39, Jun. 2008.
- I. Colak et al., "Review of multilevel voltage source inverter topologies and control schemes," Energy Convers. Manage., vol. 52, pp. 1114-1128, 2011.
- [4] J. Rodriguez et al., "Multilevel converters: An enabling technology for high-power applications," Proc. IEEE, vol. 97, no. 11, pp. 1786–1817, Nov. 2009. [5] J. Rodriguez et al., "A survey on neutral-point-clamped inverters," IEEE Trans. Ind. Electron., vol. 57, no. 7, pp. 2219–2230, Jul. 2010.
- S. Gui-Jia, "Multilevel DC-link inverter," IEEE Trans. Ind. Appl., vol. 41, no. 3, pp. 848-854, May/Jun. 2005
- P. Fang Zheng, "A generalized multilevel inverter topology with self voltage balancing," IEEE Trans. Ind. Appl., vol. 37, no. 2, pp. 611–618, Mar./Apr. 2001.
- J. A. Ferreira, "The multi-level modular DC converter," IEEE Trans. Power Electron., vol. 28, no. 10, pp. 4460-4465, Oct. 2013.
- K. Ilves et al., "A new modulation method for the modular multilevel converter allowing fundamental switching frequency," IEEE Trans. Power Electron., vol. 27, no. 8, pp. 3482-3494, Aug. 2012.
- [10] W. Yong and W. Fei, "Novel three-phase three-level-stacked neutral point clamped grid-tied solar inverter with a split phase controller," IEEE Trans. Power Electron., vol. 28, no. 6, pp. 2856-2866, Jun. 2013.
- [11] Y. Yuanmao and K. W. E. Cheng, "A family of single-stage switchedcapacitor- inductor PWM converters," IEEE Trans. Power Electron., vol. 28, no. 11, pp. 5196-5205, Nov. 2013.
- [12] P. Roshankumar et al., "A five-level inverter topology with single-DC supply by cascading a flying capacitor inverter and an H-bridge," IEEE Trans. Power Electron., vol. 27, no. 8, pp. 3505-3512, Aug. 2012.
- N. A. Rahim et al., "Transistor-clamped H-bridge based cascaded multilevel inverter with new method of capacitor voltage balancing," IEEE Trans. Ind. Electron., vol. 60, no. 8, pp. 2943-2956, Aug. 2013.
- [14] I. Abdalla et al., "Multilevel DC-link inverter and control algorithm to overcome the PV partial shading," IEEE Trans. Power Electron., vol. 28, no. 1, pp. 14-18, Jan. 2013.
- [15] Z. Li et al., "A family of neutral point clamped full-bridge topologies for transformer less photo-voltaic grid-tied inverters," IEEE Trans. Power Electron., vol. 28, no. 2, pp. 730-739, Feb. 2013.
- [16] L. Jun et al., "A new nine-level active NPC (ANPC) converter for grid connection of large wind turbines for distributed generation," IEEE Trans. Power Electron., vol. 26, no. 3, pp. 961-972, Mar. 2011.
- L. Zixin et al., "A novel single-phase five-level inverter with coupled inductors," IEEE Trans. Power Electron., vol. 27, no. 6, pp. 2716–2725, Jun. 2012.
- [18] S. Mariethoz, "Systematic design of high-performance hybrid cascaded multilevel inverters with active voltage balance and minimum switching losses," IEEE Trans. Power Electron., vol. 28, no. 7, pp. 3100-3113, Jul. 2013.
- [19] E. Babaei, "A cascade multilevel converter topology with reduced number of switches," IEEE Trans. Power Electron., vol. 23, no. 6, pp. 2657–2664, Nov.
- [20] H. Belkamel, S. Mekhilef, A. Masaoud, and M. Abdel Naiem, "Novel three phase asymmetrical cascaded multilevel voltage source inverter," IET Power Electron., vol. 6, pp. 1696-1706, 2013.
- S. Mekhilef and M. N. Abdul Kadir, "Voltage control of three-stage hybrid multilevel inverter using vector transformation," IEEE Trans. Power Electron., vol. 25, no. 10, pp. 2599-2606, Oct. 2010.
- [22] J. Mei et al., "Modular multilevel inverter with new modulation method and its application to photovoltaic grid-connected generator," IEEE Trans. Power Electron., vol. 28, no. 11, pp. 5063-5073, Nov. 2013.
- [23] A. Nami et al., "A hybrid cascade converter topology with series connected symmetrical and asymmetrical diode-clamped H-bridge cells," IEEE Trans. Power Electron., vol. 26, no. 1, pp. 51–65, Jan. 2011.
- [24] S. Mekhilef et al., "Digital control of three phase three-stage hybrid multilevel inverter," IEEE Trans. Ind. Electron., vol. 9, no. 2, pp. 719–727, May 2013.
- [25] J. Mathew et al., "A hybrid multilevel inverter system based on dodecagonal space vectors for medium voltage IM drives," IEEE Trans. Power Electron., vol. 28, no. 8, pp. 3723-3732, Aug. 2013.
- [26] M. Saeedifard et al., "Operation and control of a hybrid seven-level converter," IEEE Trans. Power Electron., vol. 27, no. 2, pp. 652-660, Feb. 2012.
- P. Sung-Jun et al., "A new single-phase five-level PWM inverter employing a deadbeat control scheme," IEEE Trans. Power Electron., vol. 18, no. 3, pp. 831-843, May 2003.
- [28] S. Mekhilef and A. Masaoud, "Xilinx FPGA based multilevel PWM single phase inverter," in Proc. IEEE Int. Conf. Ind. Technol., 2006, pp. 259–264.

- [29] C. Klumpner and F. Blaabjerg, "Using reverse-blocking IGBTs in power converters for adjustable-speed drives," IEEE Trans. Ind. Appl., vol. 42, no. 3, pp. 807–816, May/Jun. 2006.
- [30] E. A. Mahrous et al., "Three-phase three-level voltage source inverter with low switching frequency based on the two-level inverter topology," Electr. Power Appl., vol. 1, pp. 637–641, 2007.
- [31] E. A. Mahrous and S. Mekhilef, "Design and implementation of a multi-level three-phase inverter with less switches and low output voltage distortion," J. Power Electron., vol. 9, pp. 593–603, 2009.
- [32] H. W. Ping, N. A. Rahim, and J. Jamaludin, "New three-phase multilevel inverter with shared power switches," J. Power Electron., vol. 13, pp. 787–797, 2013.
- [33] S. Suroso and T. Noguchi, "Multilevel current waveform generation using inductor cells and H-bridge current-source inverter," IEEE Trans. Power Electron., vol. 27, no. 3, pp. 1090–1098, Mar. 2012.
- [34] M. F. Kangarlu and E. Babaei, "A generalized cascaded multilevel inverter using series connection of submultilevel inverters," IEEE Trans. Power Electron., vol. 28, no. 2, pp. 625–636, Feb. 2013.
- [35] C. Govindaraju and K. Baskaran, "Efficient sequential switching hybrid modulation techniques for cascaded multilevel inverters," IEEE Trans. Power Electron., vol. 26, no. 6, pp. 1639–1648, Jun. 2011.